EPJ manuscript No.
(will be inserted by the editor)

Separated cross sections in π^0 electroproduction at threshold at $Q^2 = 0.05\,\mathrm{GeV}^2/c^2$

M. Weis[1], P. Bartsch[1], D. Baumann[1], J. Bermuth[2], A. M. Bernstein[3], K. Bohinc[4], R. Böhm[1], M. Ding[1], M. O. Distler[1], I. Ewald[1], J. M. Friedrich[1,a], J. Friedrich[1], M. Kahrau[1], M. Kohl[5,b], K. W. Krygier[1], A. Liesenfeld[1], H. Merkel[1], P. Merle[1], U. Müller[1], R. Neuhausen[1], M. M. Pavan[3,c], Th. Pospischil[1], M. Potokar[4], G. Rosner[1,d], H. Schmieden[1,e], M. Seimetz[1,e], S. Širca[4,6], A. Wagner[1], and Th. Walcher[1]

A1 Collaboration

[1] Institut für Kernphysik, Johannes Gutenberg-Universität Mainz, D-55099 Mainz, Germany
[2] Institut für Physik, Johannes Gutenberg-Universität Mainz, D-55099 Mainz, Germany
[3] Laboratory for Nuclear Science, Massachusetts Institute of Technology, Cambridge, MA 02139, U.S.A.
[4] Jožef Stefan Institute, SI-1001 Ljubljana, Slovenia
[5] Institut für Kernphysik, Technische Universität Darmstadt, D-64289 Darmstadt, Germany
[6] Dept. of Physics, University of Ljubljana, SI-1000 Ljubljana, Slovenia

Received: 25 May 2007

Abstract. The differential cross sections $\sigma_0 = \sigma_T + \epsilon\sigma_L$, σ_{LT}, and σ_{TT} of π^0 electroproduction from the proton were measured from threshold up to an additional center of mass energy of 40 MeV, at a value of the photon four-momentum transfer of $Q^2 = 0.05\,\mathrm{GeV}^2/c^2$ and a center of mass angle of $\theta = 90^\circ$. By an additional out-of-plane measurement with polarized electrons $\sigma_{LT'}$ was determined. This showed for the first time the cusp effect above the π^+ threshold in the imaginary part of the s-wave. The predictions of Heavy Baryon Chiral Perturbation Theory are in disagreement with these data. On the other hand, the data are somewhat better predicted by the MAID phenomenological model and are in good agreement with the dynamical model DMT.

PACS. 25.30.Rw Electroproduction reactions – 13.60.Le Meson production

1 Introduction

Over the last two decades, neutral pion photo- and electroproduction at threshold have been established as a testing ground for Chiral Perturbation Theory. First experimental attempts at Saclay [1] and Mainz [2] to test the low energy theorem for the s-wave multipoles at threshold [3,4] initiated the development of an intense investigation of the threshold region with close cooperation between experiment and theory.

Chiral Perturbation Theory (ChPT) is the effective field theory (low energy approximation) of QCD [5,6,7,8]. The first reliable ChPT calculations of pion photoproduction in the direct threshold region showed that the old low energy theorem has to be modified, and that the s-wave prediction is a slow converging series in this calculation [9]. For two p-wave combinations, new low energy theorems were derived [10].

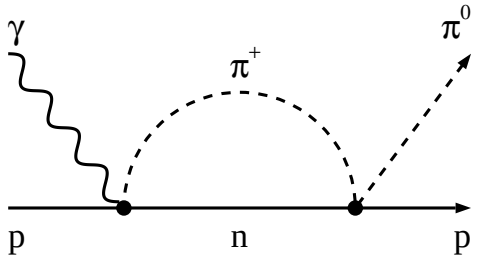

Fig. 1. The rescattering process responsible for the cusp in the π^0 s-wave amplitude at threshold.

The energy dependence of the s-wave multipoles in the $\gamma p \to \pi^0 p$ reaction has a smooth direct part and a rapidly varying (cusp) part due to a π^+ rescattering contribution shown in Fig. 1 [11,12,13]. Since the π^+ production amplitude is dominated by the additional coupling of the photon to the charge of the pion, this amplitude is much larger than the production amplitude of neutral pions, leading to a sizable unitarity cusp in the π^0 s-wave amplitude which appears in the imaginary (real) part above (below) $n\pi^+$ threshold.

The predicted cusp effect in the real part of the transverse s-wave amplitude E_{0+}, was established in photoproduction ex-

[a] *Present address:* TU München, Garching, Germany
[b] *Present address:* M.I.T., Cambridge, USA
[c] *Present address:* TRIUMF, Vancouver, Canada
[d] *Present address:* University of Glasgow, Glasgow, UK
[e] *Present address:* Universität Bonn, Bonn, Germany
Correspondence to: merkel@kph.uni-mainz.de

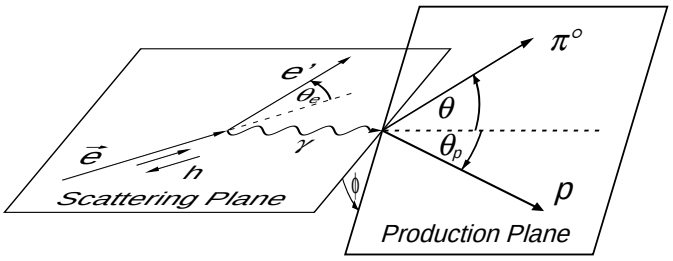

Fig. 2. Definition of the pion angles θ and ϕ in the laboratory frame.

periments at SAL [14] and MAMI [15,16,17]. While these experiments were only sensitive to the real part of this amplitude, one aim of this work is to access the imaginary part of the s-wave amplitudes. In electroproduction, this can be achieved by an out-of-plane measurement with a longitudinally polarized electron beam to access the interference cross section $\sigma_{LT'}$, which is proportional to the imaginary part of the transverse and longitudinal s-wave amplitudes E_{0+} and L_{0+}, respectively.

The second aim of the present work is to improve the experimental determination of the p-wave amplitudes. The existing electroproduction experiments with large solid angle [18, 19] covered the energy range only up to the first 4 MeV above threshold. By an extension of the experiment to an energy region of 40 MeV above threshold, where the p-waves clearly dominate, a more accurate separation of the cross sections is possible.

2 Notation and formalism

In the one photon exchange approximation the electroproduction cross section of pions can be written as (see *e.g.* [20])

$$\begin{aligned}\frac{d\sigma(\theta,\phi)}{dE_e d\Omega_e d\Omega} = \Gamma \Big(&\sigma_T(\theta) + \epsilon\,\sigma_L(\theta) + \epsilon\,\sigma_{TT}(\theta)\cos 2\phi \\ &+ \sqrt{2\epsilon(1+\epsilon)}\,\sigma_{LT}(\theta)\cos\phi \\ &+ h\sqrt{2\epsilon(1-\epsilon)}\,\sigma_{LT'}(\theta)\sin\phi\Big) \end{aligned} \quad (1)$$

with the virtual photon flux Γ, the transverse photon polarization ϵ, and the longitudinal beam polarization h. In addition, the cross sections also depend on the center-of-mass energy W (or $\Delta W = W - W_{threshold}$) and on the photon four-momentum transfer $q^2 = -Q^2 = \omega^2 - \boldsymbol{q}^2$, with the photon laboratory energy and momentum ω and $\boldsymbol{q}$.

The pion emission angles θ and ϕ are defined relative to the direction of the momentum transfer $\boldsymbol{q}$. Figure 2 shows the definition of the angles in the laboratory frame. In the following, these angles are used in the photon-proton c.m. system.

In this experiment, the photon polarization ϵ was not varied, so the differential cross section

$$\sigma_0(\theta) = \sigma_T(\theta) + \epsilon\sigma_L(\theta) \quad (2)$$

could not be separated further.

Since $\sigma_{LT'}$ is small compared to the unpolarized cross section, it is useful to define the asymmetry $A_{LT'}(\theta)$ to minimize systematic errors:

$$A_{LT'}(\theta) = \frac{\sigma^+ - \sigma^-}{\sigma^+ + \sigma^-} = \frac{\sqrt{2\epsilon(1-\epsilon)}\,\sigma_{LT'}(\theta)}{\sigma_T(\theta) + \epsilon\,\sigma_L(\theta) - \epsilon\,\sigma_{TT}(\theta)} \quad (3)$$

where σ^+ and σ^- are the differential cross sections for $\phi = 90^\circ$ with beam polarization parallel and antiparallel to the beam direction, respectively.

In the threshold region, all multipole amplitudes with angular momentum $l \geq 1$ are negligible. The cross sections can be further decomposed in s- and p-wave multipoles as

$$\begin{aligned}\sigma_T(\theta) &= p/k_\gamma \left(A + B\cos\theta + C\cos^2\theta\right), \\ \sigma_L(\theta) &= p/k_\gamma \left(A' + B'\cos\theta + C'\cos^2\theta\right), \\ \sigma_{TT}(\theta) &= p/k_\gamma \left(F\sin^2\theta\right), \\ \sigma_{LT}(\theta) &= p/k_\gamma \left(D\sin\theta + E\sin\theta\cos\theta\right), \\ \sigma_{LT'}(\theta) &= p/k_\gamma \left(G\sin\theta + H\sin\theta\cos\theta\right), \end{aligned} \quad (4)$$

where p is the pion center of mass momentum and $k_\gamma = (W^2 - m_p^2 + q^2)/(2W)$ is the equivalent real photon energy. The angular coefficients contain two s-wave and five p-wave multipole combinations [20,21]. By measuring the helicity asymmetry with an out of plane measurement, we obtain $\sigma_{LT'}$ which is proportional to the imaginary part of $(E_{0+}^* P_5 + L_{0+} P_2^*)$.

In this energy region the p-wave multipoles are approximately real so we are directly sensitive to the imaginary part of the s-wave multipoles.

3 Experiment

The experiment took place at the three-spectrometer setup of the A1 Collaboration at MAMI (see [22] for a detailed description). It was performed and analyzed based on the same techniques described in refs. [18,19]. From Eq. 1 one can see that for a separation of the cross sections, a measurement at $\phi = 0^\circ, 90^\circ, 180^\circ$ is the best choice. A measurement at $\phi = 90^\circ$ requires out-of-plane detection.

Spectrometer B of the A1 setup can be moved out of plane up to a cartesian angle of 10° in the laboratory frame [23]. By choosing spectrometer B for the electron detection at a small forward angle, we were able to cover $\phi = 90^\circ$ up to a center-of-mass momentum of $100\,\mathrm{MeV/c}$ within three kinematical settings. In addition, four in-plane settings were chosen to separate the cross sections for $\phi = 0^\circ$ and $\phi = 180^\circ$.

Table 1 summarizes the kinematical settings including the approximative acceptance range in the center-of-mass momentum. For all settings, the four-momentum transfer of the photon was fixed to the value of $Q^2 = 0.05\,\mathrm{GeV}^2/c^2$ used in former experiments [19]. At the beam energy of $E_0 = 854.49\,\mathrm{MeV}$, adjusted to optimize the spin precession angle between polarized beam source and spectrometer setup, the photon polarization was $\epsilon = 0.933$.

The polarized electron source [24] of MAMI was run at a polarization of 75% at an average current of $5\,\mu$A. The beam polarization was determined by an elastic $H(\boldsymbol{e}, e'\boldsymbol{p})$ measurement with a focal plane polarimeter in spectrometer A to an accuracy of $\pm 5\%$ absolute. To avoid systematic errors, the beam

Table 1. Kinematical settings for the central trajectory of the spectrometers. The symbols θ_e and ϕ_e mark the in-plane and out-of-plane cartesian angles of spectrometer B. Common for all settings are $Q^2 = 0.05\,\mathrm{GeV}^2/c^2$, $\theta = 90°$, $\epsilon = 0.933$, $E_{beam} = 854.49\,\mathrm{MeV}$.

pion CMS		Spectrometer A		Spectrometer B		
p	ϕ	θ_p	p_p	θ_e	ϕ_e	p_e
$\left(\frac{\mathrm{MeV}}{c}\right)$			$\left(\frac{\mathrm{MeV}}{c}\right)$			$\left(\frac{\mathrm{MeV}}{c}\right)$
0−50		44.6°	230	16.8°	0°	652
45−85	0°	52.4°	243	16.9°	0°	662
65−100	0°	58.1°	263	17.2°	0°	662
45−85	90°	43.4°	243	16.5°	3.96°	652
65−100	90°	40.1°	263	15.4°	7.65°	652
45−85	180°	34.4°	241	16.9°	0°	662
65−100	180°	22.1°	259	17.2°	0°	662

helicity was switched stochastically with a mean frequency of 1 Hz.

A subcooled liquid Hydrogen target with a oblong shape and a length of 5 cm was used. The beam was moved across the target in a controlled way by a fast raster magnet to avoid boiling of the Hydrogen. The beam current of 5 μA corresponds to a luminosity of $L = 6.7\,\mathrm{MHz}/\mu\mathrm{barn}$. A total effective beam time of 400 h was accumulated.

Spectrometer A with a solid angle acceptance of 21 msr was used for the detection of the recoil proton, and spectrometer B with an acceptance of 5.6 msr was used for the detection of the scattered electron. The focal planes of both spectrometers were equipped with four layers of vertical drift chambers for position and angular resolution and two layers of scintillators for trigger and timing resolution. In addition, spectrometer B was equipped with a gas Cerenkov detector for the suppression of charged pions. An overall momentum resolution of $\delta p/p < 10^{-4}$ and an angular resolution of better than 3 mrad was achieved. After correction for the flight path in the spectrometers, a coincidence time resolution of 2 ns FWHM was determined.

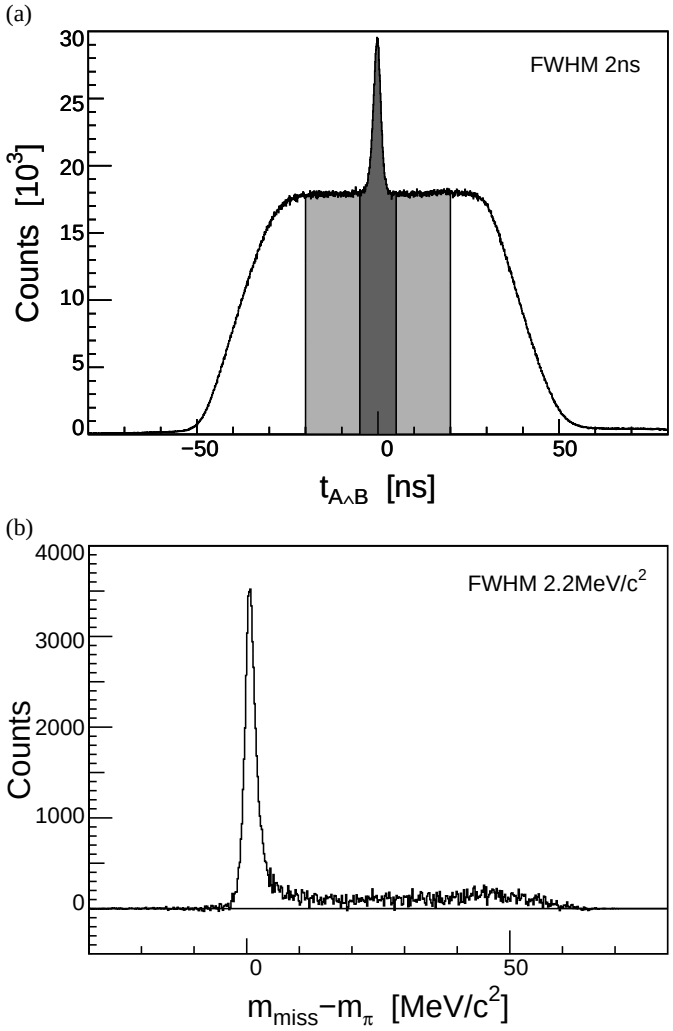

Fig. 3. Reaction identification by coincidence time (a) and background subtracted missing mass (b). The events in the dark shaded area were defined as true coincidences, while the events in the light shaded area were used to subtract the background of random coincidences.

4 Analysis and error estimation

In a first step, the electron and proton were identified by the time of flight. The coincidence time was corrected by the flight path length inside the spectrometers of about 10 m. Figure 3 (a) shows the corrected coincidence time distribution. The central peak of this distribution was used as the yield of true coincidences, while the events in the side bands were used to estimate the background of random coincidences.

The reaction $H(e,e'p)\pi^0$ was identified by a cut on the missing mass given by the four-momentum balance $m^2_{miss} = (e_{in}+p_{in}-e_{out}-p_{out})^2$. Figure 3 (b) shows the missing-mass distribution after subtraction of the background of random coincidences. The pion peak shows a missing-mass resolution of $2.2\,\mathrm{MeV}/c^2$ and a radiative tail to higher masses. The observed increase in radiative events at high masses was caused by the increase in acceptance and phase space.

The integral of the accepted phase space was calculated with the Monte Carlo method. In this calculation, all resolution and efficiency effects and radiative effects according to the formulas of ref. [27] were included. The differential cross section $\sigma(\theta,\phi)$ was extracted for several bins in W, θ, and ϕ. Since the acceptance in Q^2 and ϵ was narrow, no binning in these variables was required.

To separate the cross sections a χ^2-fit of the ϕ-dependence as given by Eq. 1 was performed for each bin in the center of mass energy W and with a cut on the pion angle of $75° < \theta < 105°$.

By the cut in θ a large fraction of events was lost. In addition, the acceptance in θ was different for each kinematical setting. To overcome these two problems, a second, model dependent method was used to separate the cross sections. In this method, the phenomenological model MAID [25] was used as parameterization of the cross section. For each event, the differential cross section was projected to the nominal kinematics at $\theta = 90°$ by

$$\sigma(90°,\phi) = \sigma(\theta,\phi)\frac{MAID(90°,\phi)}{MAID(\theta,\phi)}. \qquad (5)$$

(a) Model dependent (b) Model independent

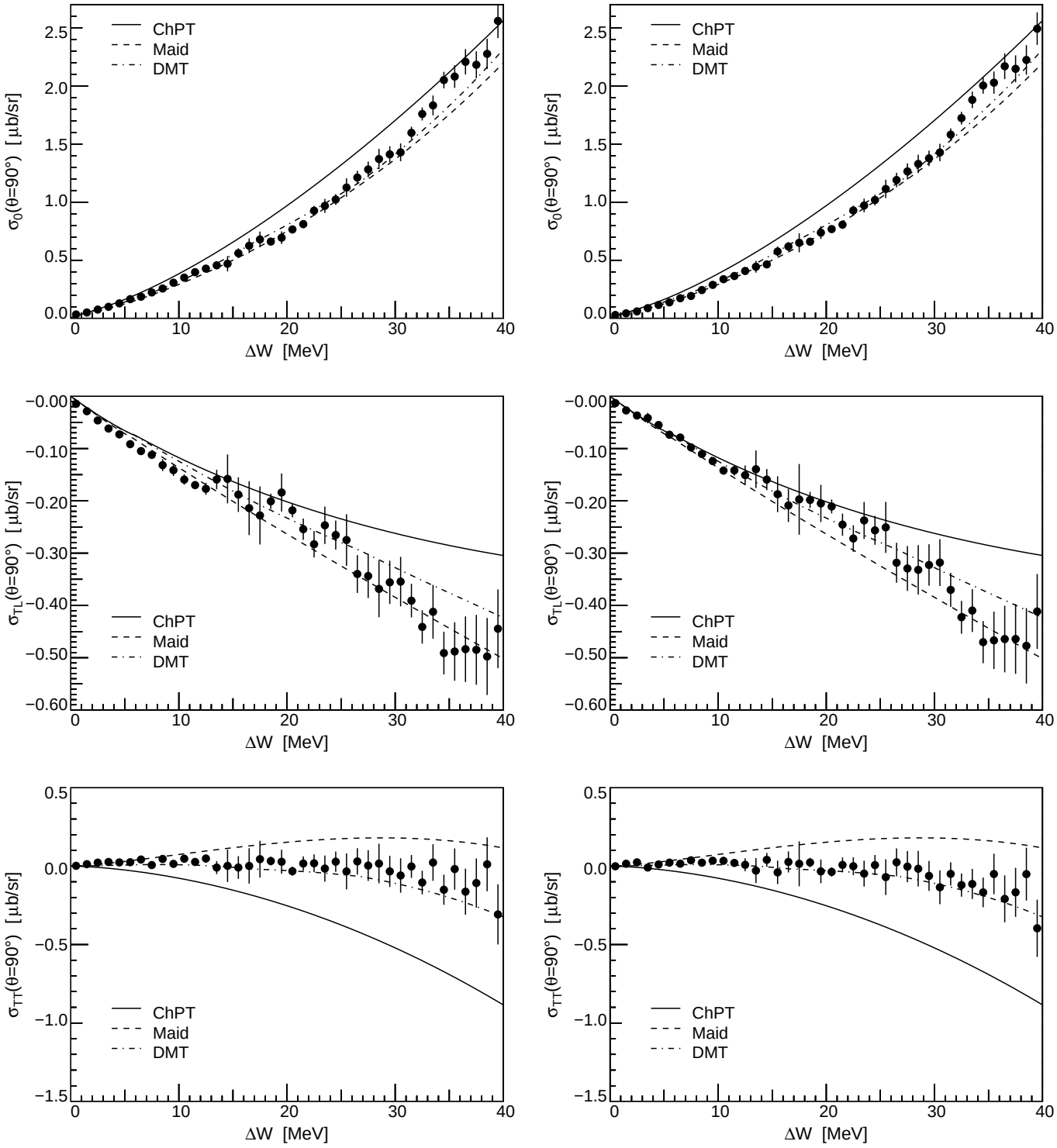

Fig. 4. The separated cross sections σ_0, σ_{LT}, and σ_{TT} at $\theta = 90°$. Column (a) shows the result with model dependent analysis using the full statistics, while column (b) shows the model independent analysis with narrow kinematical cuts. The solid line shows the calculation in HBChPT [21], the dashed line shows the phenomenological model MAID (2003 fit) [25], and the dash-dotted line shows the DMT model[26].

By this method, the statistical error could be reduced for the price of an additional model error.

The asymmetry $A_{LT'}$ was extracted by the helicity asymmetry defined in Eq. 3, including an additional background term in the denominator. The per-event-helicity and the extended ϕ acceptance were taken into account by a weight factor $h\ \sin\phi$ for each event.

The systematic errors in detection efficiency, luminosity calculation, and reaction identification could be neglected compared to the statistical error. The only notable systematic error was assigned to the first three energy bins. Directly at threshold, the extracted cross section is very sensitive to the absolute momentum calibration of the electron arm, which was calibrated to $300\,\mathrm{keV}/c$ by a measurement of elastic electron-proton scattering. For the first three bins, this results in systematic errors of 43%, 21%, and 2% respectively. For $\Delta W > 3\,\mathrm{MeV}$, the corresponding error is below 1%. For all other systematic effects an overall systematic error of 3% was determined [22].

The model error of the model dependent separation of the cross sections was estimated by varying the multipoles of the model up to $l = 1$ separately by $\pm 10\%$. This results in a model error in the extracted cross section of less than 5%. For the helicity asymmetry $A_{LT'}$ the dominant systematic error was caused by the measurement of the beam helicity h, which was known to 5%. This error is negligible compared to the statistical error.

5 Results

Figure. 4 shows the separated unpolarized cross sections σ_0, σ_{LT}, and σ_{TT}. Column (a) shows the model dependent analysis, column (b) shows the model independent analysis. Both results are clearly consistent within the error bars. The statistical advantage of the better utilization of the full data sample is compensated by the large systematic model error. Of course, the size of this error is disputable: the choice of a variation of 10% in the leading multipoles is somewhat arbitrary and the authors are convinced, that this choice is conservative. In the future, better knowledge of all multipoles can clearly improve this analysis.

Since the model dependent analysis shows that the model independent analysis is not affected by the acceptance matching, we will discuss only the model independent analysis. The data points of this analysis are compiled in Table 2.

The cross sections are compared with three theoretical calculations. The solid line in Fig. 4 shows a calculation in Heavy Baryon Perturbation Theory by V. Bernard *et al.* [21]. As already noticed in ref. [19], this calculation overestimates the cross section at $Q^2 = 0.05\,\mathrm{GeV}^2/c^2$. The reason for this might be that some of the low energy parameters of this calculation were fitted to data at a photon virtuality of $Q^2 = 0.1\,\mathrm{GeV}^2/c^2$. This value may be somewhat too large for the validity of chiral perturbation theory. Therefore, a refit of the low energy parameters to low Q^2 data might resolve some of this discrepancy. This would still leave the issue of the Q^2 dependence [19] as an unsolved problem. The more likely solution might be to carry out the ChPT calculation to higher order. The presently published calculation was carried out to order $\mathcal{O}(p^3)$ for the p-waves with some extra counter terms of higher order for the s-waves.

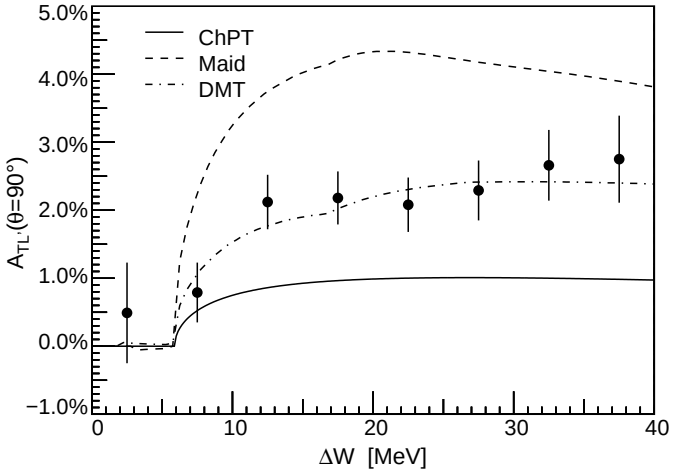

Fig. 5. The beam helicity asymmetry $A_{LT'}$ vs. center of mass energy. The solid line shows the calculation in HBChPT [21], the dashed line shows the phenomenological model MAID [25], the dash-dotted line shows the DMT model[26].

The two phenomenological models MAID [25] and DMT [26] both agree well with the unpolarized cross sections σ_0 and σ_{LT}. The small interference cross section σ_{TT}, however, is described only by the DMT model.

Table 3 and Fig. 5 give the results for the helicity asymmetry $A_{LT'}$. These data are the first experimental confirmation of the unitary cusp in an observable which is proportional to the imaginary part of the s-wave amplitudes. Unfortunately, due to the small size of this asymmetry the energy bins for this variable had to be made larger than for the unpolarized observables and a detailed determination of the shape is precluded. The data point below $n\pi^+$ threshold is consistent with the expected value of zero. $A_{LT'}$ is clearly underestimated by the HBChPT calculation [21], this is another hint that a higher order calculation is needed. The MAID model [25] overestimates $A_{LT'}$ by nearly a factor of 2. This clearly shows the necessity to include polarization observables into phenomenological fits to fix the small multipoles. The DMT model [26] is in surprising good agreement with the data. We want to stress, that this is a prediction without knowledge of the data. In this model, the threshold behavior is generated dynamically, taking the rescattering effects into account.

In all of the three models $|P_2| \gg |P_5|$, so that the primary sensitivity of $A_{LT'}$ is to the imaginary part of the longitudinal multipole L_{0+}.

6 Summary

In this experiment, we separated the cross sections σ_0, σ_{LT}, and σ_{TT} of neutral pion electroproduction at $\theta = 90°$ at a photon virtuality of $Q^2 = 0.05\,\mathrm{GeV}^2/c^2$ from threshold up to 40 MeV above threshold. The cross sections were compared with predictions of Heavy Baryon Chiral Perturbation Theory [21] and the phenomenological models MAID[25] and DMT [26]. The discrepancy between HBChPT and the data suggests

the need for higher order calculations. The phenomenological models MAID and DMT show reasonable agreement with the separated cross sections.

Simultaneous, the helicity asymmetry $A_{LT'}(90^\circ)$ was measured. This observable is sensitive to the imaginary part of the s-wave amplitudes, which was accessed for the first time by a direct measurement. This asymmetry can be described with impressive agreement by the DMT model.

This work was supported by the Collaborative Research Centers 201 and 443 of the Deutsche Forschungsgemeinschaft (DFG) and by the Federal State of Rhineland-Palatinate, and at MIT in part by the U.S. Department of Energy under Grant No. DEFG02-94ER40818. A. M. Bernstein is grateful to the Alexander von Humboldt Foundation for a Research Award. We would like to thank Ulf- G. Meißner for discussions and V. R. Brown for helpful comments on the manuscript.

References

1. E. Mazzucato *et al.*, Phys. Rev. Lett. **57**, 3144 (1986).
2. R. Beck *et al.*, Phys. Rev. Lett. **65**, 1841 (1990).
3. P. De Baenst, Nucl. Phys. B **24**, 633 (1970).
4. A. I. Vainshtein and V. I. Zakharov, Nucl. Phys. B **36**, 589 (1972).
5. S. Weinberg, Physica **A96**, 327 (1979).
6. J. Gasser and H. Leutwyler, Ann. Phys. **158**, 142 (1984).
7. J. Gasser and H. Leutwyler, Phys. Lett. **B125**, 325 (1983).
8. V. Bernard and U.-G. Meißner, Ann. Rev. Nucl. Part. Sci. **57** (2007).
9. V. Bernard, N. Kaiser, and U.-G. Meißner, Nucl. Phys. B **383**, 442 (1992).
10. V. Bernard, N. Kaiser, and U.-G. Meißner, Z. Phys. **C70**, 483 (1996).
11. G. Fäldt, Nucl. Phys. A **333**, 357 (1980).
12. V. Bernard, N. Kaiser, and U.-G. Meißner, Int. J. Mod. Phys. E **4**, 193 (1995).
13. A. M. Bernstein, Phys. Lett. B **442**, 20 (1998).
14. J. C. Bergstrom *et al.*, Phys. Rev. C **53**, 1052 (1996).
15. M. Fuchs *et al.*, Phys. Lett. B **368**, 20 (1996).
16. A. M. Bernstein *et al.*, Phys. Rev. C **55**, 1509 (1997).
17. A. Schmidt *et al.*, Phys. Rev. Lett. **87**, 232501 (2001).
18. M. O. Distler *et al.*, Phys. Rev. Lett. **80**, 2294 (1998).
19. H. Merkel *et al.*, Phys. Rev. Lett. **88**, 012301 (2002).
20. D. Drechsel and L. Tiator, J. Phys. G **18**, 449 (1992).
21. V. Bernard, N. Kaiser, and U.-G. Meißner, Nucl. Phys. A **607**, 379 (1996). Erratum A **633**, 695 (1998).
22. K. I. Blomqvist *et al.*, Nucl. Instrum. Meth. A **403**, 263 (1998).
23. M. Weis, Diploma thesis, Mainz University (1997).
24. K. Aulenbacher *et al.*, Nucl. Instr. and Meth. A **391**, 498 (1997).
25. D. Drechsel, O. Hanstein, S. S. Kamalov, and L. Tiator, Nucl. Phys. A **645**, 145 (1999).
26. S. S. Kamalov, G.-Y. Chen, S.-N. Yang, D. Drechsel, and L. Tiator, Phys. Lett. B **522**, 27 (2001).
27. L. W. Mo and Y.-S. Tsai, Rev. Mod. Phys. **41**, 205 (1969).

Table 2. The separated cross sections σ_0, σ_{LT}, and σ_{TT}. Only the model-independent results with cut $75^\circ < \theta < 105^\circ$ are given in this table.

ΔW (MeV)	$\sigma_0(90^\circ)$ (nb/sr)	$\sigma_{LT}(90^\circ)$ (nb/sr)	$\sigma_{TT}(90^\circ)$ (nb/sr)
0.5	29.5 ± 1.0	-13.2 ± 0.7	-1.4 ± 1.5
1.5	43.7 ± 0.6	-27.3 ± 0.4	14.8 ± 0.9
2.5	60.3 ± 2.0	-36.9 ± 1.4	23.6 ± 3.1
3.5	88.0 ± 14.2	-41.7 ± 10.0	-9.3 ± 22.3
4.5	115.2 ± 7.7	-55.1 ± 5.5	10.5 ± 12.1
5.5	137.7 ± 10.4	-73.7 ± 7.4	21.9 ± 16.4
6.5	172.9 ± 5.6	-79.1 ± 3.9	15.2 ± 8.7
7.5	192.9 ± 10.6	-97.9 ± 7.7	37.0 ± 16.6
8.5	243.9 ± 7.1	-110.6 ± 5.1	21.4 ± 11.2
9.5	288.4 ± 7.9	-124.0 ± 5.6	34.4 ± 12.5
10.5	337.0 ± 10.9	-142.2 ± 7.7	33.4 ± 17.1
11.5	364.2 ± 14.3	-141.7 ± 10.1	19.8 ± 22.5
12.5	407.8 ± 26.2	-151.0 ± 18.6	8.2 ± 41.3
13.5	443.9 ± 50.5	-139.7 ± 35.8	-28.8 ± 79.5
14.5	464.1 ± 25.6	-159.5 ± 20.2	40.0 ± 44.1
15.5	575.5 ± 42.6	-187.4 ± 34.3	-40.1 ± 75.0
16.5	618.3 ± 38.3	-208.8 ± 31.7	26.4 ± 67.0
17.5	650.4 ± 81.7	-197.2 ± 67.6	14.3 ± 143.1
18.5	659.9 ± 22.3	-198.4 ± 15.4	23.0 ± 29.8
19.5	738.0 ± 54.6	-205.0 ± 35.5	-33.8 ± 75.8
20.5	768.0 ± 22.6	-210.8 ± 13.3	-37.2 ± 29.4
21.5	806.0 ± 35.5	-245.5 ± 21.1	7.4 ± 47.2
22.5	928.0 ± 42.1	-272.0 ± 25.4	-1.0 ± 57.0
23.5	971.1 ± 59.2	-237.6 ± 35.4	-48.1 ± 82.4
24.5	1018.3 ± 46.2	-256.4 ± 27.6	6.1 ± 64.3
25.5	1113.4 ± 79.0	-250.8 ± 48.9	-70.6 ± 113.6
26.5	1190.2 ± 61.8	-318.4 ± 38.2	24.0 ± 88.9
27.5	1264.3 ± 69.3	-329.4 ± 42.9	-3.6 ± 99.6
28.5	1329.0 ± 79.2	-331.9 ± 47.2	-16.9 ± 113.4
29.5	1376.6 ± 66.4	-322.7 ± 39.6	-62.8 ± 95.1
30.5	1427.1 ± 75.0	-318.1 ± 44.7	-135.2 ± 107.4
31.5	1580.4 ± 54.0	-370.3 ± 32.6	-49.9 ± 73.9
32.5	1722.7 ± 54.7	-422.6 ± 31.4	-121.1 ± 73.8
33.5	1879.8 ± 71.2	-409.8 ± 41.0	-114.3 ± 96.2
34.5	2003.2 ± 70.2	-470.2 ± 40.3	-167.6 ± 94.7
35.5	2027.6 ± 95.3	-466.7 ± 54.8	-50.5 ± 128.6
36.5	2169.0 ± 110.7	-464.3 ± 63.7	-209.0 ± 149.4
37.5	2146.9 ± 115.9	-464.2 ± 66.6	-167.4 ± 156.3
38.5	2223.2 ± 127.1	-477.1 ± 72.1	-51.4 ± 168.3
39.5	2492.2 ± 140.1	-411.6 ± 71.7	-396.6 ± 182.6

Table 3. The helicity asymmetry $A_{LT'}$ at $\theta = 90^\circ$.

ΔW (MeV)	$A_{LT'}$ (%)
2.5	0.49 ± 0.74
7.5	0.79 ± 0.44
12.5	2.12 ± 0.40
17.5	2.18 ± 0.39
22.5	2.08 ± 0.40
27.5	2.29 ± 0.44
32.5	2.66 ± 0.52
37.5	2.75 ± 0.64